
Article:
Zhang, B. and Marshall, M.B. orcid.org/0000-0003-3038-4626 (2019) Investigating material removal mechanism of an Al-Si base abradable coating in labyrinth seal system. Wear, 426-427. pp. 239-249. ISSN 0043-1648

https://doi.org/10.1016/j.wear.2019.01.034

Title

Investigating material removal mechanism of Al-Si base abradable coating in labyrinth seal system

Author

Boxiu Zhang, PhD Student, Mechanical Engineering, University of Sheffield

Matthew Marshall, Professor, Mechanical Engineering, University of Sheffield

Corresponding author contact information

Boxiu Zhang

S35 Velocity One, 3 Solly St,

Sheffield, UK,

S1 4DF

Other author contact information

Matthew Marshall

Department of Mechanical Engineering,

Sir Frederick Mappin Building,

Mappin Street,

Sheffield, UK,

S1 3JD

Abstract

Labyrinth seal systems are used in aero-engines to seal the clearance between turbine blades and the surrounding engine casing, and an understanding of the wear mechanism by which this occurs is necessary to achieve better sealing performance. In this work a series of tests are conducted on a high-speed test rig capable of fin tip speeds of 100m/s. The mechanism by which the fin removes material is investigated over a range of incursion rates, with force and temperature measurements along with high-speed imaging recorded in each case. Surface examination and sectioning is also performed using microscopy post-test. The wear mechanism was found to be incursion rate dependent. At low incursion rates (0.02μm/pass), abradable material is removed via a cyclic process, where it is first compacted in the worn groove, until ductility is lost and material fractures away from the surface of the groove. At high incursion rates (2μm/pass), material is extruded out of the sides of the groove forming lips, before fracturing off. This process is more efficient, with lower relative forces and temperatures. As the incursion rate increases from low to high, the mechanism shows a gradual transition, with compaction being replaced with extrusion.

1 Introduction

Abradable coatings are applied in aero-engines to seal the clearance between rotating blades and fins and the surrounding engine structure. [1, 2] This is done in order to minimise the leakage gap, with the aim of sacrificing the abradable to protect the blade [3] or fin [4]. Therefore, it is important to understand the mechanism by which the blade or fin removes the abradable in order to apply the most appropriate coating at a given engine stage, and to achieve a maximized working performance. Previously, investigations by Fois and Watson [5-9] have focused on the material removal mechanism between compressor blades and abradable coatings, resulting in this contact being well understood. The removal mechanism of compressor blades depends on material factors such as blade and abradable material, as well as operational aspects such as tip speed and incursion rate. Generally, at low incursion rates, the material removal mechanism tends to one of adhesive/abrasive wear, while at high incursion rates a cutting mechanism prevails. [5,6,9]. These observations are in line with Borel [10], who postulated that a compress release mechanism occurs at low incursion rate, with chip formation ahead of the blade as the rate increases. In contrast to those studies present for compressor blades, the material removal mechanism between abradables and sealing fins has received limited attention. Delebarre et al. investigated the contact between a sealing fin and an Al-Si abradable material [11-13], using a modified test arrangement comprising of abradable material thermally sprayed onto a rotating drum. In their studies, cyclic behaviour in terms of force and displacement was observed at low incursion speed [11]; with a more continual wear mechanism prevailing as this rate increased [13]. Similarly, Zhang and Marshall investigated a nickel based abradable system retained within an Inconel 718 honeycomb structure in contact with a nickel alloy based fin, using a more conventional static abradable sample combined with a fin mounted in a rotating disc. Tests were undertaken at an intermediate incursion speed, with cyclic material removal and sparking occurring in some tests [14]. Following on from these investigations, this study aims to investigate the material removal mechanism of a fin seal more fully over a range of incursion conditions. In line with previous tests, whilst in an aero-engine application the fin seal comprises of a full ring, a short segment is used here. However as previously identified [14], similar wear mechanisms are developed in this test arrangement to those found in an aero-engine, and the arc of contact is developed on the flat abradable sample as the test progresses. Tests are conducted using an M601MS abradable in combination with Ti-6Al-4V fins, with this representing a typical combination found in many aero-engine applications. Through a combination of in-situ measurement techniques, along with post-test analysis of the worn abradable and fin samples, the wear mechanism is investigated. This paper introduces the results of this study, with the objectives of identifying the abradable material removal mechanism, and evaluating the influence of different incursion conditions on the wear behaviour of the aforementioned sealing system.

2 Methodology

2.1 Test Samples

The abradable used in this study is M601NS, with a R15Y hardness of 82. M601NS is a typical thermally sprayed abradable coating, consisting of aluminium, silicon, and a polymer dislocator, and is used in fin sealing systems in the low-pressure turbine stage of an aero-engine [15]. In this study, the M601NS abradable material is deposited on the centre of a 80mm×80mm stainless steel backing plate (Figure 1a) by a thermal spraying process, with a final thickness of 3mm achieved. Figure 1b shows the fin samples used in this study which 30mm in length, 3mm thick, with a 1.2mm taper at the fin tip. These fins are made of Ti-6Al-4V alloy, and have been shown to achieve a good working performance when combined with the aluminium based abradables used in the engine.

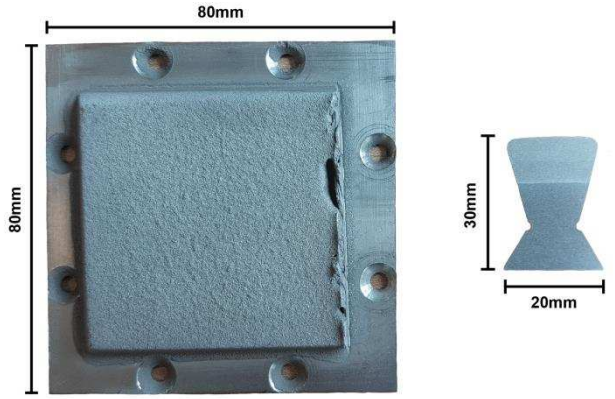

Figure 1 Abradable and fin samples

2.2 Test Procedure and Camera Arrangement

Tests are conducted on the same test rig (Figure 2) that has previously been used for a variety of studies on aero-engine abradable systems, and specifically in the previous investigation of honeycomb reinforced nickel based fin seals [14]. As shown in the figure, the test rig consists of a disc driven by a machine tool spindle, with an axial stage providing relative motion between the test samples. In a typical incursion test, the fin sample to be investigated is mounted into the rotating disc using clamps. The disc also contains a dummy fin, 2mm shorter than the test fin but of the same mass, mounted in opposition to the test fin in order to provide balancing. The abradable sample is mounted below the test fin on top of the axial stage, and after setting the spindle rotation speed and vertical stage speed, an incursion event occurs between the two test samples. During the incursion test, the force and temperature generated at contact point is measured using a dynamometer (Type 9327C, Kistler Instruments Ltd., London, UK) and pyrometer (thermometer CTLaser M3, Micro-epsilon, Koenigbacher, Germany) respectively. With respect to the pyrometer, this is focused in the middle of the wear scar generated by the fin on the abradable sample, and used to obtain a single point temperature measurement, indicative of the overall thermal behaviour of the test. In addition to the instrumentation used previously, in this case a stroboscopic imaging system in line with the fin / abradable contact has also been included in the test arrangement. A light gate is used to trigger the system, and images are recorded of the contact between the fin and blade throughout the test, with the aim of identifying the material removal mechanism.

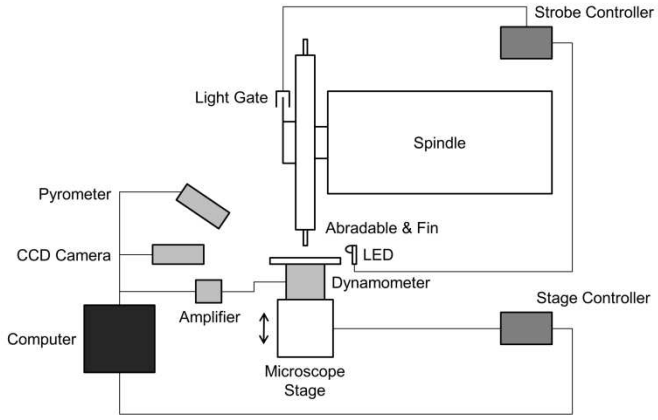

Figure 2 Test rig schematic diagram

2.3 Data analysis

As noted, in this study force and temperature data is captured using a dynamometer and pyrometer respectively. All of the instrumentation on the test rig is controlled via a purpose written Labview programme, with data files from each instrument saved individually in a text format with a timestamp. The raw force data outputs are processed into two data sets comprising normal and tangential forces by extracting the peak values of force from each strike. As previously identified [14], no further compensation is required for the force measurements with respect to the vibration behaviour of the test rig. Conversely, as the pyrometer outputs a data file containing temperature at a given time step, no further processing is needed in this case. As highlighted, in both cases measured outputs are on a common time base. However, previous research [14] has identified that as the arc of contact increases with time as a consequence of the test arrangement, rub length is a more appropriate base to analyse the data from, and as such the following equation has been applied to convert the experimental outputs from a time base to one of rub length. The equation for rub length is a follows:

$$\mathbf{L} = \sum_{i=1}^{n} \cos^{-1}\left(\frac{\boldsymbol{r - incursion\ rate \times i \times 10^{-6}}}{\boldsymbol{r}}\right) \times \boldsymbol{r}$$

where L is counted total rub length, r is the fin disk radius and i is the number of pass.

Figure 3a shows an example un-processed image taken using the stroboscopic measurement system. As shown in the figure, shadowing is apparent in the image, obstructing some of the features present, and occurs as a consequence of diffusion of the LED light source. In particular, the shadow makes it hard to see the abradable profile clearly, and identify material removal from the surface. As such, in order to post-process the images, the shadows were removed using the 'imlincomb' function in the Matlab Image processing toolbox, with a coefficient of 2 selected when applying the function. As shown in Figure 3b, this function enhances the image brightness and in the areas experiencing shadowing, thus allowing the material removal mechanism to be accurately identified.

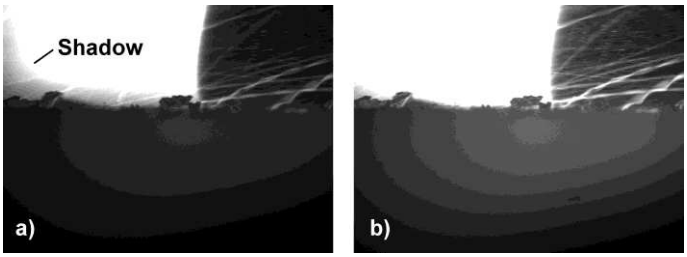

Figure 3 Enhanced bottom camera frame: a) original frame, b) enhanced frame

2.4 Post-test Analysis

Images of the fin and worn groove were photographed post-test using a SLR camera (Nikon D5200 with 18-55mm f/3.5-5.6G DX VR lens, Nikon Co., Tokyo, Japan). The worn groove is also investigated using surface microscopy in order to gain a more detailed insight of the surface topography. Alongside this, the abrdable samples are also sectioned centrally perpendicular to the wear track, in order to investigate any transfer layers present, along with compaction of the abradable sample. In all cases the microscope used in this study is a Carl Zeiss Imager A1.M optical microscope with 5.0x zoom-in coefficient and the SEM used is Hitachi Tabletop Microscope TM3030. It should be noted that as the worn surface of the abradable is not flat, multiple images are recorded of the sample at different focal depths, and then stitched together to form a single focused image. Figure 4 shows an example of this process, where three raw images having different focused depths are laid out from bottom (left) to surface (right). In order to get the fully focused image, all the focused areas in each image are selected and extracted, and then combined into one single image using Adobe Photoshop.

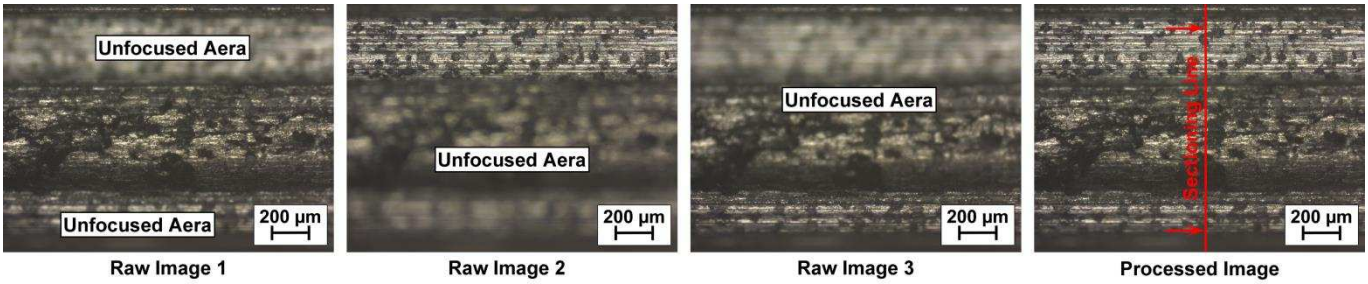

Figure 4 Post-processing of microscope images from the wear track

2.5 Test Matrix

As highlighted previously, fin tip speed and incursion rate are dominant test parameters with respect to the wear mechanism of abradable sealing systems, and in particular incursion rate has been found to have the strongest influence [5]. The upper tip speed of the aforementioned test rig is 200 m/s, however as previous studies [5-9] have identified that representative wear mechanisms occur at speeds of 100m/s, the lower speed was selected for this investigation in order to maximise the quality of images recorded using the stroboscopic imaging system. As stated, the primary aim of this study is to investigate the effect of incursion rate on material removal mechanism. As such, initially three different incursion speeds, 3.1µm/s, 93.1µm/s and 310µm/s, were selected corresponding to incursion rates of 0.02µm/pass, 0.6µm/pass, 2µm/pass. These three incursion rates were selected as they have been previously identified as engine representative [6, 8], with the upper rate corresponding to running and handling of the engine, and lower and intermediate cases simulating light and heavy in flight incursion events. In the case of investigations into compressor sealing systems, these incursion rates have also been found to give a full spectrum of wear mechanisms. In all tests the incursion depth is set at 2000µm, with this being deemed sufficient for the wear mechanisms to fully develop and data to be captured for complete analysis. Table 1 lists the test matrix for this study. As shown in the table, all tests are repeated twice with the camera system first focused on the fin leading edge (L) and then the trailing edge (T), in order to fully investigate material removal, with this achieved by changing the time delay on the stroboscopic system depending on which area is to be investigated in a given test.

Test Code	Fin	Abradable	Tip Speed [m/s]	Incursion Speed [µm/s]	Incursion Rate [µm/pass]	Incursion Depth [µm]
Ti64-0.02-L	Ti-6Al-4V	M601NS	100	3.1	0.02	2000
Ti64-0.02-T	Ti-6Al-4V	M601NS	100	3.1	0.02	2000
Ti64-0.6-L	Ti-6Al-4V	M601NS	100	93.1	0.60	2000
Ti64-0.6-T	Ti-6Al-4V	M601NS	100	93.1	0.60	2000
Ti64-2-L	Ti-6Al-4V	M601NS	100	310.0	2.00	2000
Ti64-2-T	Ti-6Al-4V	M601NS	100	310.0	2.00	2000

Table 1 Test matrix

3 Results

3.1 Abradable & fin profile after test

Figure 5 shows the test samples from the outlined matrix. As shown, whilst details such as thermal damage can be observed in the fin samples at the leading and trailing edges, as the groove in the abradable is relatively narrow, it is hard to identify detailed features from the wear track. However, with reference to the equation for calculating rub length, the expected length of the arc of contact is a product of the blade tip radius, and should wear occur, this arc length in practice reduces. As such the length of fins before and after test was measured and the change calculated (Figure 6a), and compared to the arc length on the abradable samples (Figure 6b) with an arc length of 40.3mm corresponding to a zero wear case. As shown by the figures, in the case of the low incursion rate, fin wear was highest with a corresponding lowest value of groove length in the abradable sample. In this case, thermal damage was also the most observable on the fin sample. As incursion rate increases, fin length change and thermal damage then progressively reduces, with the worn groove in the abradable similarly increasing in length. Contrasting back to studies on compressor blades [5], these results also highlight that large-scale adhesion of abradable material to the fin is not taking place, as fin length change and abradable arc length are consistent, and also that the overall mechanism is consistent given the similarities between the repeat tests for the leading and trailing edge camera positions.

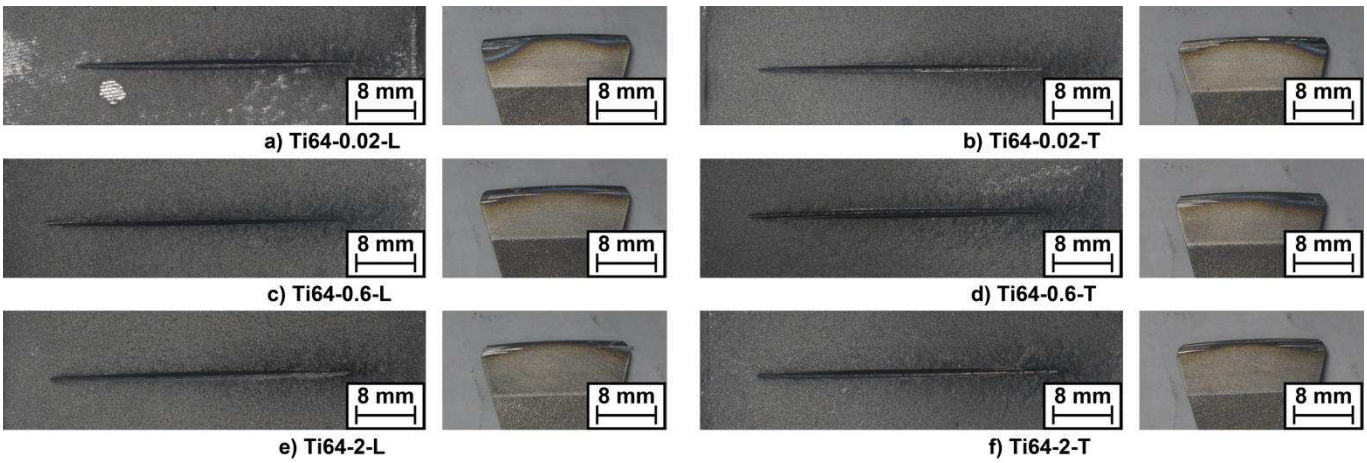

Figure 5 Abradable and fin samples post-test a) 0.02 microns per pass (leading edge set), b) 0.02 microns per pass (trailing edge set), c) 0.6 microns per pass (leading edge set), d) 0.6 microns per pass (trailing edge set), e) 2 microns per pass (leading edge set), f) 2 microns per pass (trailing edge set)

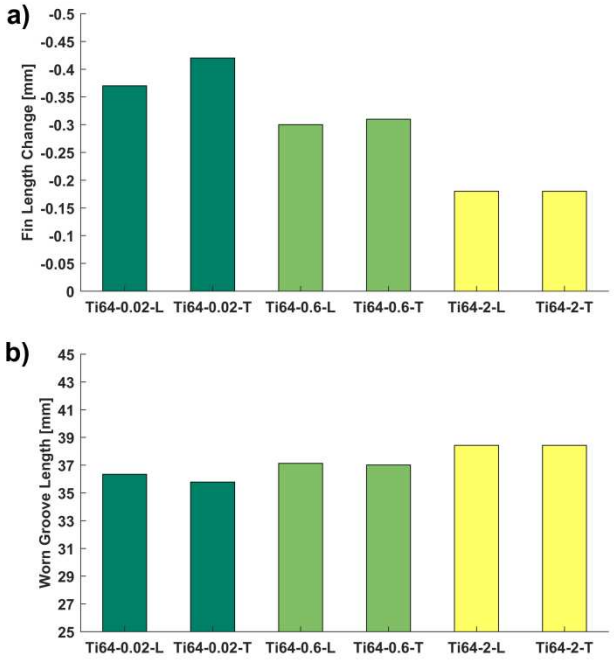

Figure 6 Bar chart of a) Fin length change, b) worn groove length

3.2 Force & temperature

Figure 7 shows the processed force and temperature results for all tests. As previously stated, the tests were repeated twice at each condition in order to investigate both the leading and trailing edge of the fin using the stroboscopic imaging system. For example, tests Ti64-0.02-L and Ti64-0.02-T are individual tests with the same test condition, with the latter case representing a repeat, as the differing camera position has no impact on the other data acquisition systems.

As shown in Figures 7a & b, at an incursion rate of 0.02µm/pass, both tests exhibit cyclic behaviour with periodic peaks in force and temperature repeats. It is also noticeable that overall normal force gradually rises during the test, before stabilising towards the end. In the case of the repeat test (Figure 7b), it is also interesting to note that in this case whilst the forces are similar, spikes in temperature are higher. The cyclic behaviour observed is also similar to that seen in previous studies [14], with the spike in temperature following the rise in force. It should also be noted that no common frequency was found to exist in the observed force and temperature cycles, and it is not coincident with either the blade passing frequency or harmonics of the rig, and is therefore thought to be as a consequence of the fin-abradable interaction. Moving to the intermediate incursion rate (Figures 7c & d), whilst cyclic behaviour is still evident to a degree in the temperature data, it is now broadly absent in the force data, which is relatively stable and does not increase through the test. Finally at the high incursion rate (Figures 7e & f), whilst variation in force and temperature is observed during the tests, no cyclic behaviour is observed.

Figure 8 shows the average normal force, tangential force and temperature at each incursion rate tested, with error bars included to show the variation between the two repeat tests at each condition. As shown in the figure, the average forces at the middle incursion rate have the highest values, followed by those at the high incursion rate, and finally the low incursion rate. This is combined with a slight increase in temperature between the low incursion rate tests, and those performed at the intermediate and high value, with this increase still being significantly lower than the observed peaks during the identified cyclic behaviour at low incursion rate. In line with previous studies on compressor blades [5], these results indicate a move to a more efficient material removal mechanism as the incursion rate increases, as the force and temperature are not increasing in line with the fin load (incursion rate per pass). Further, the increase in tangential force in the absence of increased normal force has also been found to be indicative of a cutting mechanism as a consequence of the increased force ratio [6], and this will be investigated further in the subsequent sections.

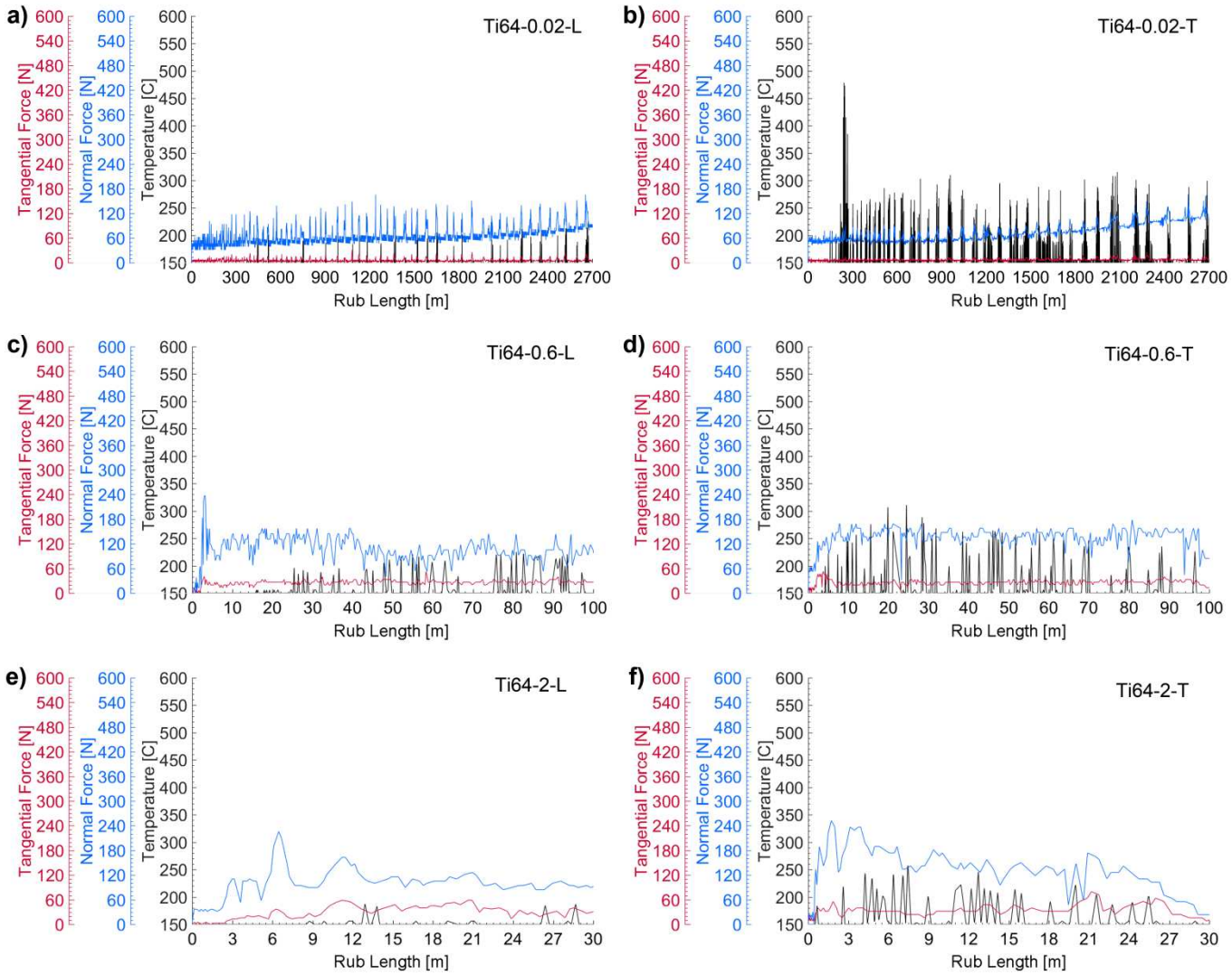

Figure 7 Force and temperature results of test with incursion rate at a) 0.02 microns per pass (leading edge set), b) 0.02 microns per pass (trailing edge set), c) 0.6 microns per pass (leading edge set), d) 0.6 microns per pass (trailing edge set), e) 2 microns per pass (leading edge set), f) 2 microns per pass (trailing edge set)

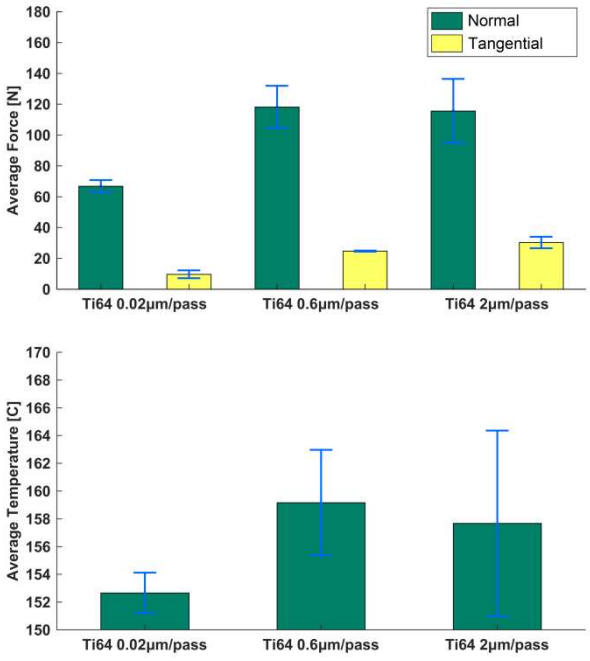

Figure 8 Average a) force and b) temperature for the tests

3.3 Stroboscopic Imaging

Figure 9 shows images from the stroboscopic camera set-up, placed in line with the blade strike. It should be noted that these images are the same perspective as the images shown in Figure 3 but cropped to highlight the material extruding mechanism. Due to this, the fin edge is not shown in Figure 9b and c since it sits outside of selected area. Images are sampled from the data set of each incursion investigated, with the selection chosen to highlight material removal behaviour. As previously noted, images are recorded from the trailing edge of the fin contact, with the fin passing from left to right in the images shown. These images were chosen as no evidence of chip formation ahead of the fin was found on the images from the leading edge, and the images below show sequentially how the material removal mechanism occurs. As shown in the figure, at all incursion rates material is extruded from the wear track and builds up at the side of the contact. In terms of duration, unsurprisingly this process follows the incursion rate, with it undergoing a shift in scale with respect to time base, comparable to that seen for incursion rate (i.e. a factor of approximately 100 between 0.02 and 2 microns per pass), corresponding with the material removed per pass and available for extrusion. It is also apparent that the maximum height of extruded material changes with this peaking at the upper incursion condition. Finally, as shown at all incursion rates, the extruded material breaks off and is removed periodically during the incursion.

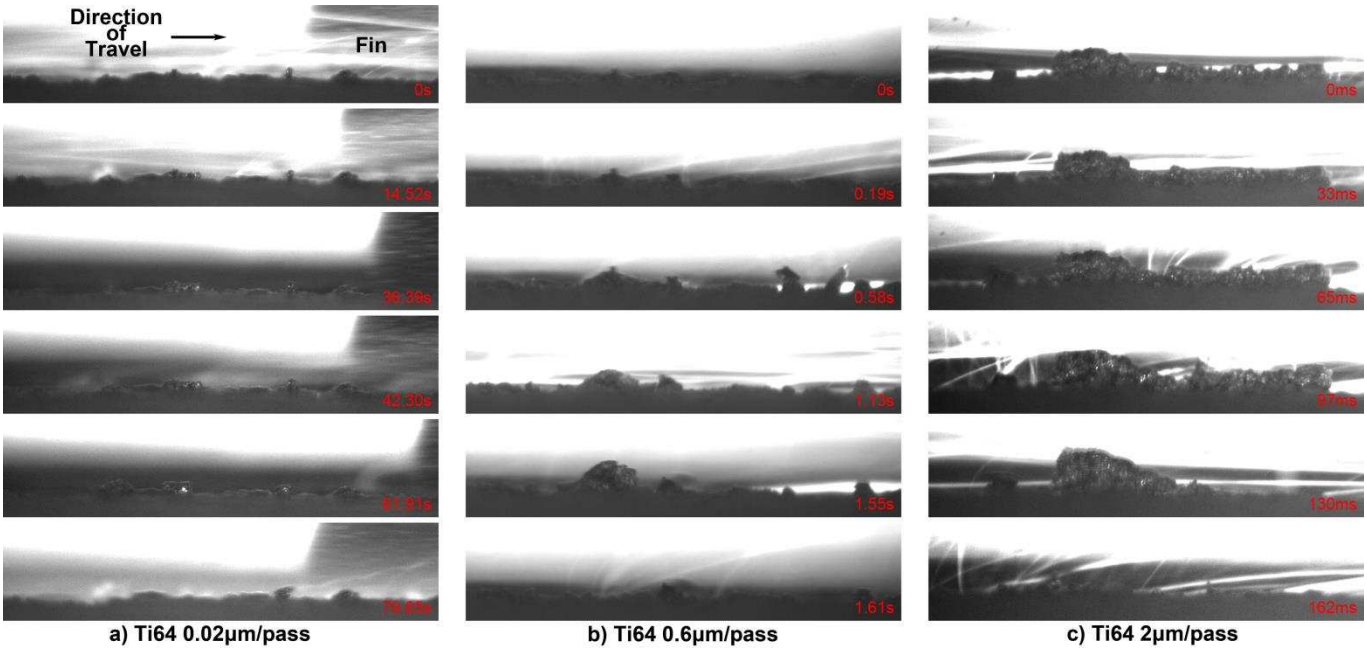

Figure 9 Frames extracted from the stroboscopic imaging results with the incursion rate at a) 0.02 microns per pass, b) 0.6 microns per pass, c) 2 microns per pass.

From the images taken with the camera, the area behind the fin can also be investigated. As shown in Figure 10, chips of material are evident behind the fin, and are either fractured pieces of the extruded material, or else being released from within the wear track via a compress/release mechanism as suggested for compressor blade – abradable interactions by Borel [10]. As with the extruded material, it is also noticeable that more of this fractured debris exists as the incursion rate increases, with the particles moving from tiny flakes at low incursion rates, to large pieces as the rate increases. Finally, it is interesting to note, that whilst this apparent cyclic behaviour of extrusion and fracture is evident to some degree at all incursion rates, cyclic forces and temperatures were only recorded for the low incursion rate case, with sparks also most evident in the low incursion rate images in Figure 9. This implies an additional material removal mechanism takes place at this incursion rate.

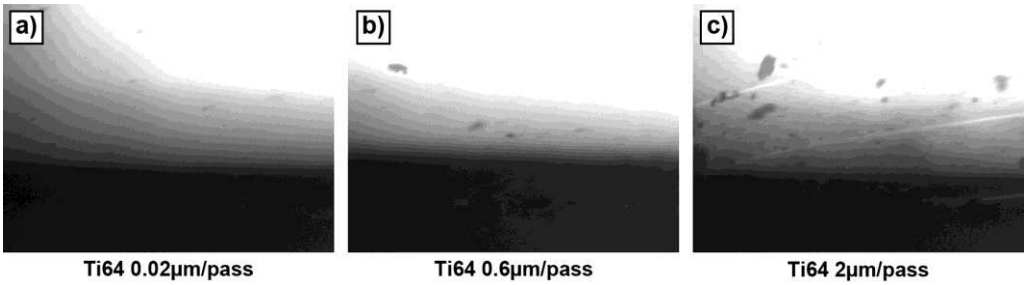

Figure 10 Images of ejected debris captured with the imaging system a) 0.02 microns per pass, b) 0.6 microns per pass, c) 2 microns per pass.

3.4 Worn groove surface microscope images

Figures 11 and 12 show the microscope and SEM images taken from the centre of the worn groove surfaces. As highlighted in the figures, the morphology of the worn groove surfaces can be classified in two ways. Firstly, areas exist with compacted abradable material, which in places has formed a near shiny solid layer. This morphology is present at the low incursion rate (Figures 11a & b), and also to a degree at the intermediate rate (Figures 11c & d). As shown by the SEM image in Figure 12a, used to further investigate these compacted regions, a layered structure with cracking is evident, indicating it is transient in nature. These consolidated regions are also interspersed with areas where the compacted material appears to have fractured off, exposing new abradable material. Such regions are further detailed in the SEM image in Figure 12b, where the sprayed structure of the abradable is evident. Conversely at the high incursion rate (Figures 11e & f), and also in part at the intermediate rate, the abradable surface appears well fractured and close to the as sprayed condition. These results fit well with those presented in Figures 9 and 10, and

indicate that the ejected particles observed at the low incursion rate are a combination extruded material from the sides of the groove that has been fractured off, as well as material released from the consolidated layer at the bottom of the groove. In this latter case, the compaction and release of material from the bottom of the worn groove also appears to align with the cyclic behaviour observed in terms of force and temperature, with a similar phenomenon previously recorded for grit tipped compressor blades [7] where compaction and release / sparking occurred. Conversely, the clean cut morphology of the groove surface at high incursion rate, supports the view that the identified ejected material is broken off from that extruded at the sides, with the intermediate rate containing a mixture of the two mechanisms identified.

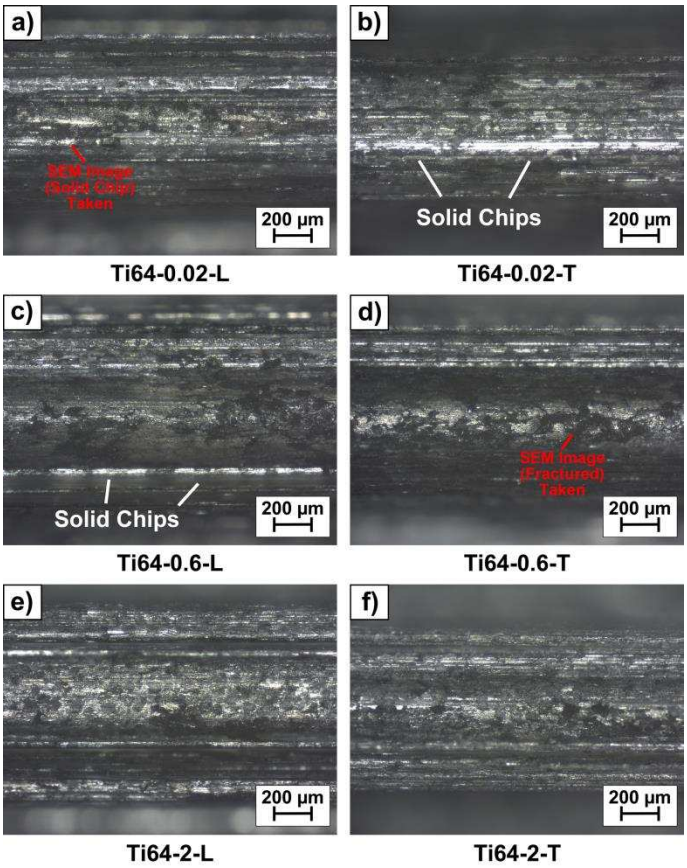

Figure 11 Worn groove surface microscope images a) 0.02 microns per pass (leading edge set), b) 0.02 microns per pass (trailing edge set), c) 0.6 microns per pass (leading edge set), d) 0.6 microns per pass (trailing edge set), e) 2 microns per pass (leading edge set), f) 2 microns per pass (trailing edge set)

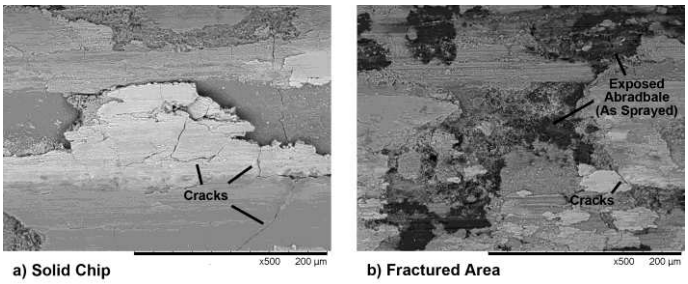

Figure 12 Worn groove surface SEM images for the low incursion rate test (0.02 microns per pass) a) Smeared Area, b) Fracture Surface

4 Discussion

The above tests further identified the material removal mechanism observed for fins, with both extrusion of material to the side of the worn groove, as well as material release from the bottom of the groove identified. However, in particular at low incursion rates the process is not yet fully characterised. For example, as highlighted in Figure 7a & b normal force continues to rise through the test, and when combined with the compaction of the groove surface identified at these incursion rates in Figure 11a & b, it is unclear as to whether the test is stable, or the abradable is progressively compacting and a more catastrophic failure, as seen in some nickel based abradable systems [9] may ultimately occur. Therefore in the following section a limited series of tests of varying rub length and depth will be performed at the low incursion rate condition, in order to understand the stability of the mechanism identified, before the overall mechanisms observed are more fully discussed.

4.1 Variable Rub Length Test

As introduced above, to determine whether the abradable material is compacted during the low incursion rate experiments, additional tests were conducted. Table 2 shows the additional tests performed at an incursion rate of 0.02 microns per pass, with the incursion depth stepped in 500micron intervals. These tests were performed on the same rig using samples manufactured to the same specification as previously. In this case, the stroboscopic imaging system was not used, as the focus was to investigate the force and temperature behaviour, along with the worn groove morphology post-test as a function of test duration.

Test Code	Fin	Abradable	Tip Speed [m/s]	Incursion Speed [µm/s]	Incursion Rate [µm/pass]	Incursion Depth [µm]	Rub Length [m]
100-0.02-500	Ti-6Al-4V	M601NS	100	3.1	0.02	500	338
100-0.02-1000	Ti-6Al-4V	M601NS	100	3.1	0.02	1000	955
100-0.02-1500	Ti-6Al-4V	M601NS	100	3.1	0.02	1500	1755
100-0.02-2000	Ti-6Al-4V	M601NS	100	3.1	0.02	2000	2702

Table 2 Designed testing parameters for variable rub length tests

Full results from the tests are shown in the Appendix, with a focus on the groove morphology and cutting efficiency presented here. As shown in Figure 13a-d, the surface of the worn groove appears stable throughout the test. As previously noted, the surface is comprised of consolidated areas, interspersed by cracked and fractured areas where new abradable material is exposed, with this mechanism appearing cyclic where consolidation-cracking-fracture-exposure of new material occurs repeatedly in a locality during the test. Further, Figure 13e-f show the corresponding sections of the abradable samples, taken perpendicular to the rub track at the central point of the specimen. As shown in the figures, the consolidated layer is limited to the near surface of the rub track, and shows no increase in severity throughout the test. Overall these results highlight the mechanism as stable, but do not provide an explanation for the increasing normal force observed at low incursion rate.

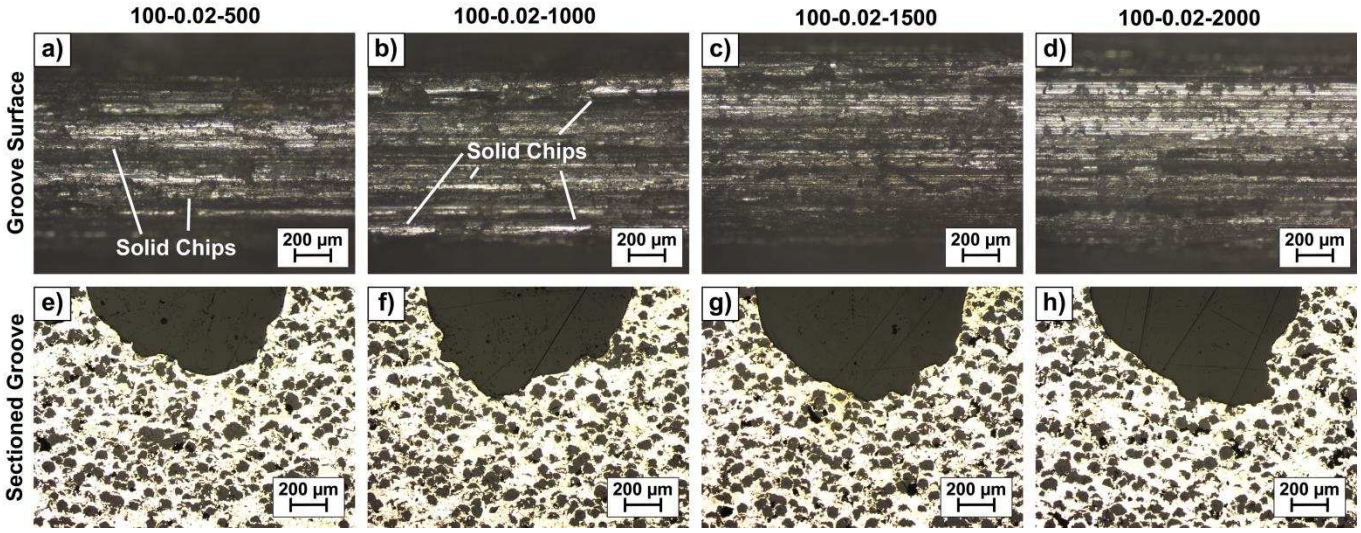

Figure 13 Images of the worn groove at each rub depth tested a) surface image 500 microns, b) surface image 1000 microns, c) surface image 1500 microns, d) surface image 2000 microns, e) sectioned image 500 microns, f) sectioned image 1000 microns, g) sectioned image 500 microns, h) sectioned image 2000 microns

The efficiency of the material removal mechanism present in terms of the energy consumed by the rub, and whether it is changing, can be estimated from the force results [16]. As shown in the equation below, in this case it is assumed that the energy used equates to the mechanical energy recorded by the dynamometer only, and other energy dissipation modes such as thermal are ignored. Whilst this is a simplification and likely underestimation, it is a useful tool for comparison, and also by considering the volume of material theoretically removed at a given point in the rub, allows the energy consumed per cubic millimeter of material removed to be determined. The following equation has therefore been used:

$$E_{total} = E_{cutting} + E_{feeding} = \int F_{tangential}\ dRL + \int F_{normal}\ dID$$

where RL is rub length and ID is incursion depth.

As shown in Figure 14, whilst the energy does rise with test duration for the test at 0.02 microns per pass, this increase is less significant when compared to the changes seen overall with incursion rate, and also when normalized with respect to volumetric material removal. In this latter case, it is interesting to note that as the sample is flat the arc length increases during the test as the fin penetrates the abradable sample and the volume of removed material grows. Given that the test at low incursion rate appears to have a rubbing mechanism, compared to an extrusion dominated mechanism for the tests at intermediate and high incursion rate, this suggests that the increasing normal force observed, may be as a consequence of the rubbing mechanism present in this particular case.

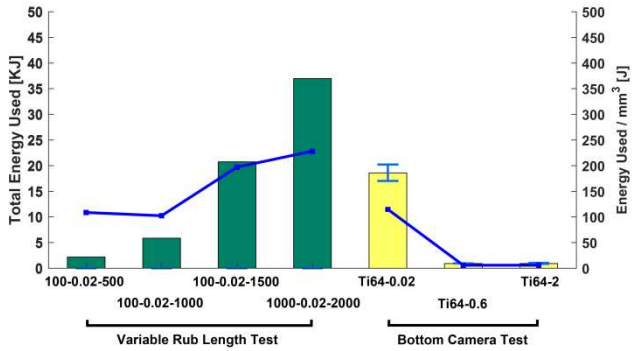

Figure 14 Estimated total energy for the incursion event and energy used to remove a unit volume of material

4.2 Increasing normal force

As highlighted in the previous section, the increasing normal force occurring for the low incursion rate tests is not as a consequence of increasing compaction of the abradable sample, as has been seen previously in work on nickel based abradables interacting with a blade form [7]. Indeed, in previous studies with compressor blades [9], whilst a rubbing mechanism has been identified at low incursion rates, normal forces have generally been stable throughout the test. However, as shown in Figure 15, the contact area for a blade is significantly different to that of a fin, particularly in the case where rubbing is occurring and the contact is likely to be less dominated by the leading edge. As shown, as the incursion depth progresses from 50microns to 500 microns, whilst the blade achieves full contact quickly upon the test commencing and maintains thereafter, the contact area of the fin (depicted by the dark red area) continues to grow as the overall incursion depth increases. Further, if a rubbing and compaction / push back mechanism exists, this also means that the normal force will grow over the duration of a fin test in line with contact area.

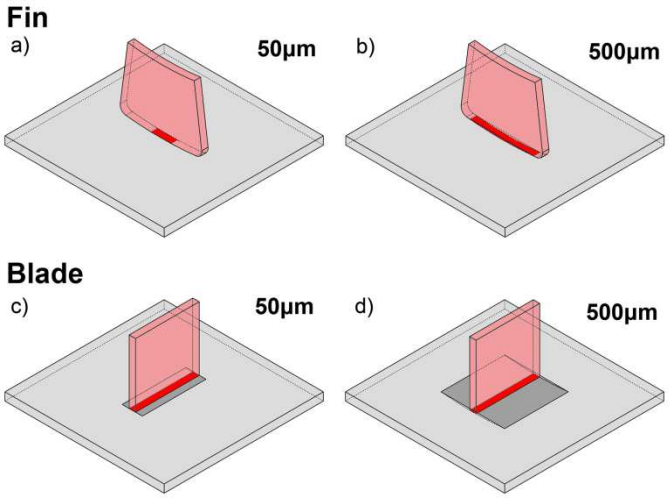

Figure 15 Contact area of fin and blade with abradables during incursion test a) fin test at 50µm, b) fin test at 500 µm, c) blade test at 50µm, d) blade test at 500µm

Up until the fin is fully engaged (at an arc length of 16.30mm, and incursion depth of 0.32mm), the contact arc at a given point in the test can be calculated using the following equation:

$$l_{arc} = \cos^{-1}\left(\frac{r - incursion\,rate \times i \times 10^{-6}}{r}\right) \times r$$

where r is disc radius with fin attached (102.5mm), and i the pass number completed by the fin during the test. Using these assumptions, Figure 16 shows a theoretical prediction of normal force based on arc length compared to the measured value. The theoretical line has been calculated by taking an average of the normal force from the period of the test where the fin is fully engaged (and the force becomes broadly constant), and then scaling it based on the percentage of the fin contacting the abradable surface at a given point in the test. As shown, form agreement between the two curves is reasonable, suggesting that variable contact area during the rubbing event offers a good explanation of the observed increasing normal force in the low incursion rate tests.

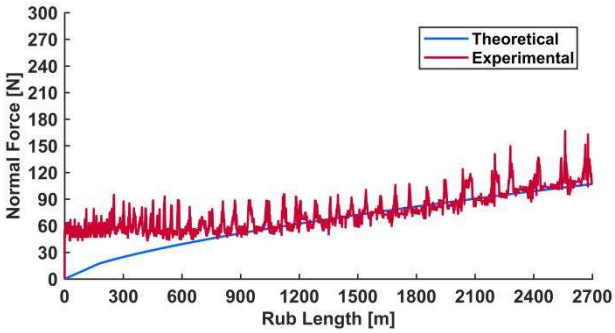

Figure 16 Theoretical and real normal force result comparison

4.3 Abradable material removal mechanism

With the reason behind the increasing normal force seen at low incursion rate identified, the overall mechanisms present can now be more full discussed. From the force, temperature, and stroboscopic imaging results for the tests samples, along with the post-test microscope evaluation of the rub tracks, it is clear that the material removal mechanism for fins is incursion rate dependent. This is in line with observations by Debarre et al. [11-13] who noted cyclic behaviour with respect to force and displacement measurements at low incursion rate. As shown by the schematic in Figure 17, at low incursion rate the fin rubs the surface of the abradable, leading to both extrusion of material at the sides wear track, and more importantly compaction of material in the bottom of the track. Forces then rise, along with temperatures (Figure 7a & b), until this compacted material is locally fractured and released (Figures 10 & 13), with the process then repeating leading to the observed cyclic nature of the incursion

event. When released, this debris is at high temperature resulting in the observed sparks (Figure 9), and thermal damage also occurs to the fin at the leading and trailing edges. This material removal process is also similar to that previously observed for honeycomb based abradable linings [14], where sparking occurred at test conditions where consolidation and fracture of the abradable surface occurred.

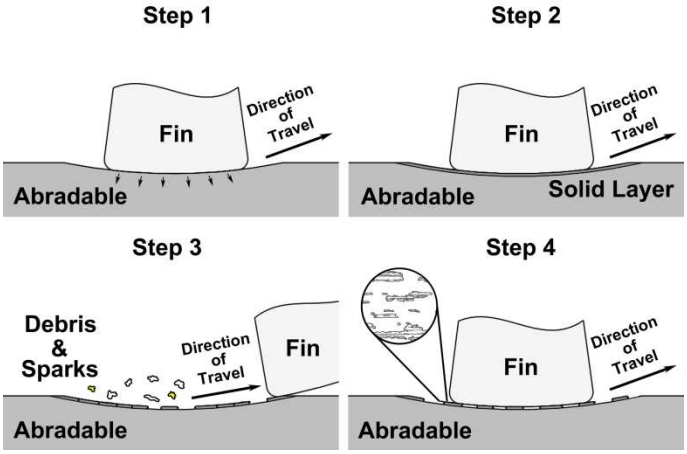

Figure 17 Schematic diagram of abradable material removal mechanism at low incursion rate

Comparatively, Figure 18 shows a schematic of the material removal mechanism identified at high incursion rates. As shown in the figure, material is extruded from the side of the groove before periodically detaching, with this behaviour best highlighted by the images shown in Figure 9. As shown in Figures 7 & 8, this mechanism is more efficient that than seen at low incursion rate, with the abradable surface well fractured (Figure 11e & f). However, whilst this does reflect an improved mechanism for fins, it is not directly comparable to the cutting mechanism observed for blades [6], where chip formation occurs ahead of the blade and material removal analogous to a turning process occurs. Although, in many ways this result is not surprising given the blunt nature of a fin compared to a blade, the overall improvement in abradable performance is still reflective of the behaviour identified as 'cutting' by Debarre et al. [11-13]. Finally, as the incursion rate transitions from low to high incursion rate, as highlighted in Figure 9, a gradual move from rubbing and cyclic fracture to extrusion occurs, with a corresponding improvement in the efficiency of material removal.

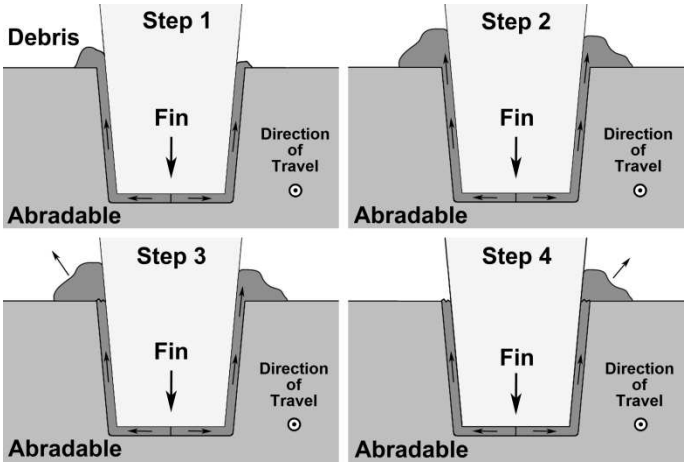

Figure 18 Schematic diagram of abradable material removal mechanism at high incursion rate

5 Conclusion

This study investigated the material removal mechanism of a M601NS abradable interacting with a Ti-6Al-4V fin. The results identified the following with respect to the wear mechanisms present:

- The wear mechanisms present, whilst having some similarities to those seen for blades interacting with abradables, possess significant differences as a consequence of the different geometry that the fin possesses compared to a blade.
- At low incursion rate a cyclic mechanism occurs, with material compacted by the fin, leading to force and temperature spikes as this material ultimately fractures and is released. Limited extrusion also occurs at the edges of the worn grooves in the abradable.
- At high incursion rates, the material removal mechanism is more efficient, with material extruded to the side of the fin contact, before fracturing off. In terms of volumetric material removal, forces and temperatures are also relatively low.
- As the incursion rate increases from low to high, a gradual transmission occurs between the two mechanisms, with extrusion appearing the more dominant material removal mode at n incursion rate of 0.06 microns per pass.

Reference

[1] M. Dorfman, U. Erning, J. Mallon, Gas turbines use abradable coatings for clearance-control seals, 2002, Sealing Technology, Vol. 2002-1, pp. 7–8. https://doi.org/10.1016/S1350-4789(02)80002-2

[2] T. N. Rhys-Jones, The use of thermally sprayed coatings for compressor and turbine applications in aero engines, 1990, Surface and Coatings Technology, Vol. 42-1, pp. 1-11. https://doi.org/10.1016/0257-8972(90)90109-P

[3] D. Sporer, A. Refke, M. Dratwinski, M. Dorfman, Sulzer Metco, I. Giovannetti, M. Giannozzi, M. Bigi, New high-temperature seal system for increased efficiency of gas turbines, 2008, Sealing Technology, Vol. 2008-10, pp. 9-11. https://doi.org/10.1016/S1350-4789(08)70517-8

[4] P. Dowson, M. Walker, A. Watson, Development of abradable and rub-tolerant seal materials for application in centrifugal compressors and steam turbines, 2004, Sealing Technology, Vol. 2004-12, pp.5–10. https://doi.org/10.1016/S1350-4789(02)80002-2

[5] N. Fois, J. Stringer, J and M. Marshall, Adhesive transfer in aero-engine abradable linings contact, 2013, Wear, Vol. 304, No. 1-2, pp. 202-210. Wear 304 (2013) 202–210. https://doi.org/10.1016/j.wear.2013.04.033

[6] N. Fois, M. Watson, J. Stringer, M. Marshall, An investigation of the relationship between wear and contact force for abradable materials. 2014, Proceedings of the Institution of Mechanical Engineers, Part J: Journal of Engineering Tribology, Vol. 229, No. 2, pp. 136-150. https://doi.org/10.1177/1350650114545139

[7] M. Watson, N. Fois, M. Marshall, Effects of blade surface treatments in tip–shroud abradable contacts, 2015, Wear, Vol. 338-339, pp. 268-281. https://doi.org/10.1016/j.wear.2015.06.018

[8] N. Fois, M. Watson, M. Marshall, The influence of material properties on the wear of abradable materials, 2016, Proceedings of the Institution of Mechanical Engineers, Part J: Journal of Engineering Tribology. https://doi.org/10.1177/1350650116649528

[9] M. Watson, M. Marshall, Wear mechanisms at the blade tip seal interface, 2018, Wear, Vol. 404–405, pp. 176-193. https://doi.org/10.1016/j.wear.2018.03.009

[10] M.O. Borel, A.R.Nicoll, H.W.Schlapfer, R.K.Schmid, The wear mechanisms occurring in abradable seals of gas turbines, 1989, Surface and Coatings Technology, Vol. 39/40, pp.117–126. https://doi.org/10.1016/0257-8972(89)90046-7

[11] C. Delebarre, V.Wagne, J.Y.Paris, G.Dessein, J.Denape, J.Gurt-Santanach, An experimental study of the high speed interaction between a labyrinth seal and an abradable coating in a turbo-engine application, 2014, Wear, Vol. 316, pp. 109-118. https://doi.org/10.1016/j.wear.2014.04.023

[12] C. Delebarre, V.Wagne, J.Y.Paris, G.Dessein, J.Denape, J.Gurt-Santanach, The wear mechanisms occurring in a labyrinth seal-abradable contact depending on the incursion depth parameter, 2016, Mechanics & Industry, Vol. 17. https://doi.org/10.1051/meca/2015118

[13] C. Delebarre, V.Wagne, J.Y.Paris, G.Dessein, J.Denape, J.Gurt-Santanach, Tribological characterization of a labyrinth-abradable interaction in aturbo engine application, 2017, Vol. 370-371, pp. 29-38. https://doi.org/10.1016/j.wear.2016.11.007

[14] B. Zhang, M. Marshall, Investigating the application of a honeycomb abradable lining in the turbine stage of an aero-engine, 2018, Tribology International, Vol.125, pp.66-74. https://doi.org/10.1016/j.triboint.2018.04.013

[15] Oerlikon Metco, Material product data sheet - Aluminum silicon polymer thermal spray powders. 2016.

[16] D. Stephenson, J. Agapiou, Metal cutting theory and practice. 3rd Edition, 2016. Boca Raton: CRC, Taylor & Francis group, pp.402-404.

Appendix I – Abradable and fin profile after test of additional variable rub length test

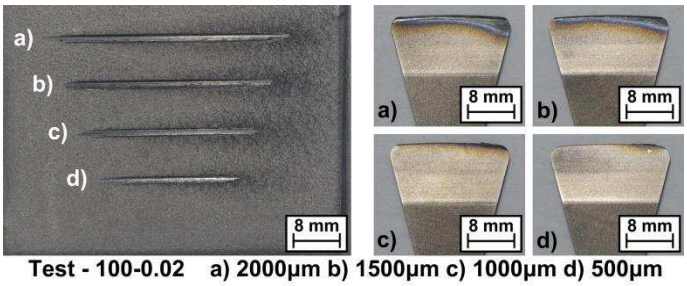

Test - 100-0.02 a) 2000µm b) 1500µm c) 1000µm d) 500µm

Appendix II – Force and temperature results of additional variable rub length test